Stability of CuZnOAl$_2$O$_3$/HZSM-5 and CuFe$_2$O$_4$/HZSM-5 catalysts in dimethyl ether steam reforming operating in reaction-regeneration cycles

Lide Oar-Arteta, Aingeru Remiro*, Jorge Vicente, Andrés T. Aguayo, Javier Bilbao, Ana G. Gayubo

Chemical Engineering Department, University of the Basque Country

P. O. Box 644, 48080, Bilbao, Spain. Phone: +34 946 015361. Fax: +34 946 013 500.

*Email: aingeru.remiro@ehu.es

Abstract

The study focuses on the regenerability of bifunctional catalysts prepared with different metallic functions (CuZnOAl$_2$O$_3$ and CuFe$_2$O$_4$ spinel) and HZSM-5 zeolite (SiO$_2$/Al$_2$O$_3$ = 30) as the acid function. These catalysts have been employed for H$_2$ production in the steam reforming of dimethyl ether in a fluidized bed reactor, operating in reaction-regeneration cycles. The regeneration of the catalysts was carried out by combustion in air (temperature range of 315-500 ºC) of the deposited coke, in order to establish: i) the coke combustion temperature required for recovering the activity of the metallic and acid functions; and ii) the kinetic behaviour of the catalysts after removing the coke deposited on the metallic function and after the complete removal of coke. The coke combustion is selective and at 315 ºC only the coke deposited on the metallic sites is burned, whereas 500 ºC are required to remove the coke deposited on the zeolite. It has been proven the higher stability of the catalyst with CuFe$_2$O$_4$ spinel metallic function, which allows operating uninterruptedly under reaction-regeneration cycles, since it recovers its activity after regeneration at 500 ºC (necessary for the combustion of the coke deposited on the zeolite). The catalyst with CuZnOAl$_2$O$_3$ metallic function, which is more active than the Cu-Fe spinel for the dymethyl ether steam reforming, deactivates irreversibly at 500 ºC due to Cu sintering.

Keywords: Hydrogen, DME steam reforming, CuFe$_2$O$_4$ spinel, HZSM-5 zeolite, deactivation, regeneration.

1. Introduction

The increasing demand on energy requires the valorization of alternative sources to oil (coal, natural gas, biomass) in order to obtain fuels and petrochemical industry commodities. In this context, the H_2 plays a crucial role both as a clean fuel and as a reactant. H_2 can be used directly or by means of an hydrogenated intermediate (H_2 carrier) that can be transformed *in situ* into H_2 by reforming for its use in hydrogen fuel cells [1,2].

Amongst the compounds available as H_2 vectors in fuel cells, dimethyl ether (DME) has received considerable attention because of its advantages (even over methanol) such as high hydrogen content (13 wt% vs. 12.5 wt% of methanol), low toxicity (harmless), gas-like properties, liquid-storage density, and the infrastructure available for its handling (similar to that for LPG) [3,4]. Furthermore, the steam reforming of DME (SRD) can also proceed at low temperatures (300-400 ºC temperature range), only slightly higher than those required for the steam reforming of methanol (SRM) [5-8]. Moreover, DME can be synthesized from biomass resources (bio-DME), via the syngas obtained from biomass gasification [9], and furthermore, DME synthesis by co-feeding CO_2 with syngas in a single reaction step is considered a key process for CO_2 sequestration [10-12].

The SRD proceeds over bifunctional catalysts, via hydrolysis of DME (over an acid function, Eq 1), followed by the steam reforming of MeOH (SRM) (over a metallic function, Eq 2), resulting in the overall reaction given by Eq 3:

$$(CH_3)_2O + H_2O \Leftrightarrow 2CH_3OH \tag{1}$$

$$CH_3OH + H_2O \Leftrightarrow 3H_2 + CO_2 \tag{2}$$

$$(CH_3)_2O + 3H_2O \Leftrightarrow 6H_2 + 2CO_2 \tag{3}$$

Additionally, other reactions take place which decrease H_2 production, such as reverse water gas shift (r-WGS, Eq 4) and DME decomposition (Eq 5) reactions:

$$CO_2 + H_2 \Leftrightarrow H_2O + CO \tag{4}$$

$$(CH_3)_2O \rightarrow CH_4 + H_2 + CO \tag{5}$$

Moreover, the formation of hydrocarbons can take place at temperatures above 300 ºC on strong acid sites [13,14] and significant coking may occur on the catalyst surface due to the dehydrogenation of the hydrocarbons formed [15].

Consequently, suitable bifunctional catalyst formulations and operating conditions are required for attaining high DME conversion and H_2 selectivity, by avoiding the formation

of CO (poison for the anodic catalyst in PEM fuel cells) and CH_4 as byproducts. The most used acid function for the catalyst preparation is the γ-Al_2O_3 [5,16-21], but due to its low acidity requires a high temperature (300-400 ºC) for the DME hydrolysis (Eq 1), which favors DME decomposition (Eq 5) and reverse WGS reaction (Eq 4). A function of higher acidity, such as HZSM-5 zeolite, allows obtaining high H_2 yields at temperature values 100 ºC under those required with γ-Al_2O_3, but its excessive acidity may favor HCs formation [6,14,22]. A moderation of the HZSM-5 zeolite acidity by means of an alkaline treatment with NaOH has been proven to be effective for avoiding the hydrocarbon production [14].

The $CuZnOAl_2O_3$ (CZA) formulation has been extensively used as metallic function of the catalyst for the SRD [6,13-16,23,24]. This metallic function restricts the reaction temperature due to Cu sintering above 300 ºC, which is a handicap for its use together with γ-Al_2O_3 as acid function. In order to attenuate Cu sintering, other metallic functions include Cu-CeO_2 [25-27] and Cu-Ni [21]. Ni addition diminishes Cu sintering, as it improves the surface dispersion and strengthens the interaction between Cu and γ-Al_2O_3. In order to carry out the SRD at higher temperature, the use of CuM_xO_4 spinels of Fe ($CuFe_2O_4$) and other metals (M= Al, Co, Cr, Ga, Mn, Ni) has been proposed [5,17-20,28-32]. Kameoka et al. [32] found that the sintering of copper particles was significantly inhibited after H_2 reduction at 600 ºC of $CuFe_2O_4$ spinel, and Shimoda et al. [29,30] achieved the regeneration of a $CuFe_2O_4$/γ-Al_2O_3 catalyst for the SRD under an oxidant atmosphere, by means of coke removal and reconstruction of a new $CuFeAlO_4$ spinel even more active than the fresh one.

Catalysts based on noble metals, such as Pd, Pt and Ru, have also been used in the SRD since they present some advantages such as higher thermal stability and longer-term stability than Cu-based catalysts [33]. Nevertheless, most of the studies with noble metals show low activity and selectivity in the SRM when compared to Cu-based catalysts, given that noble metals promote the decomposition of MeOH instead of its direct reforming [34]. Pt/Al_2O_3 and Ru/Al_2O_3 show a relatively high DME conversion, although high production of CH_4 is obtained [35]. The formation of CH_4 (up to 25 %) notably diminishes (down to 7 %) by mixing Pt/Al_2O_3 catalyst with Pd/Al_2O_3 without loss of hydrogen production [7]. In the SRD, Pd based functions provide higher yields of byproducts (especially CO) than Cu-based catalysts, requiring from subsequent water-gas shift (WGS) step in order to purify the H_2 stream [25].

Catalysts with CZA metallic function and HZSM-5 zeolite acid function (pure or alkali treated) achieve high activity and selectivity in the SRD process at low temperature (~ 300 ºC) [14,36,37]. However, they suffer from a slight deactivation due to coke deposition, thus requiring a regeneration step by coke combustion. The regenerability of this type of

catalysts, employed in the SRD, has not been analyzed before in bibliography, but it is supposed to present some problems due to Cu sintering above 320 ºC.

In this work, the regenerability of bifunctional catalysts based on Cu metallic functions (both CZA conventional function and copper-ferrite spinel $CuFe_2O_4$) and on HZSM-5 zeolite as acid function (pure or alkali treated in order to diminish its acidity) has been compared. For this purpose, successive reaction-regeneration cycles have been carried out under different operating conditions both in the reaction step (in order to obtain catalysts with different deactivation levels) and the regeneration step, which consists of coke combustion in air at low (315 ºC) and high (500 ºC) temperature. All the deactivated and regenerated catalysts have been characterized (analysis of the metallic properties and TPO of the coke) in order to correlate the results obtained in the kinetic runs with the properties of the catalysts.

2. Materials and Methods

2.1 Catalyst preparation

The bifunctional catalysts were prepared by wet physical mixing of $CuZnOAl_2O_3$ (CZA) or copper-ferrite spinel ($CuFe_2O_4$) as metallic function, and commercial HZSM-5 zeolite pure (HZ30) or alkali treated (AHZ30) as acid function.

The CZA metallic function with Cu/Zn/Al nominal atomic ratio of 4.5:4.5:1.0 was prepared by the conventional coprecipitation method which gave satisfactory results for SRM [38,39]. The corresponding nitrates ($Cu(NO_3)_2 \cdot 3H_2O$, $Zn(NO_3)_2 \cdot 6H_2O$ and $Al(NO_3)_3 \cdot 9H_2O$, (*Panreac*, 99 %)), were precipitated with Na_2CO_3 at pH= 7.0 and 70 ºC under the conditions established in previous papers [36,40]. The resulting solid was washed (as often as required for the total removal of alkaline cations), dried in two steps (at room temperature for 12 h and then at 110 ºC for another 12 h) and calcined (*Thermicon P Heraeous, SA* muffle) at 325 ºC for 3 h, following a heating ramp of 5 ºC min^{-1} in order to transform the metallic carbonates (precursors) into oxides.

Copper-ferrite spinel was prepared by the sol-gel method from a citrate complex precursor, according to Shimoda et al. [30]. An aqueous solution of Cu and Fe nitrates was stirred for 2 h at 60 °C and then, the citric acid was added and kept stirring for one more hour. After this, it was heated up to 90 °C to eliminate all the remaining water. Subsequently, the solution was placed into a muffle furnace, maintained at 150 °C for 30 minutes in order to decompose the citric acid and at 300 °C for 5 h, until the oxide powder was formed. Finally, the resulting spinel was calcined at 900 °C for 10 h.

The ZSM-5 zeolite (SiO_2/Al_2O_3=30), denoted HZ30, was supplied in ammonium form by Zeolyst International. The modified ZSM-5 zeolite (AHZ30) was prepared by alkaline treatment (with a solution of NaOH 0.4 M at 80 ºC for 300 min) of the commercial zeolite following the method described in previous papers [14,41]. The acid form of the parent zeolite and the alkali treated zeolite was obtained by calcination in a muffle furnace (*Thermicon P Heraeus, SA*) at 550 ºC for 3 h, following a previously described heating sequence [14].

The wet physical mixing of both functions (acid and metallic) for obtaining the bifunctional catalysts consisted in slowly adding the acid function to 1 L of distilled water under continuous stirring at room temperature, until a well dispersed suspension was obtained. The metallic function was then added and stirred for 30 min. The homogeneous mixtures obtained were centrifugated to separate the solid, which was dried, firstly at room temperature for 24 h and subsequently in an oven at 110 °C for another 24 h. The powder obtained was calcined for 3 h (at 325 °C for the CZA metallic function and at 550 ºC for the $CuFe_2O_4$ spinel) and subsequently pressed, ground and sieved to a particle size between 90 μm and 250 μm, which is suitable for a fluidized bed reactor.

The optimum mass ratio between the metallic and the acid function was: i) 1/1 for CZA/HZ30 and CZA/AHZ30 catalysts, as it was determined in previous work [36], and ii) 4/1 for $CuFe_2O_4$/HZ30 catalyst, due to the lower activity of the spinel for the steam reforming compared to CZA [30].

2.2. Catalyst characterization

The specific surface area of the bifunctional catalysts was determined by N_2 adsorption-desorption (*Micromeritics ASAP 2010*) employing the conventional BET method. The reduction temperature and the metallic species liable to reduction were determined by temperature programmed reduction (TPR, *Micromeritics AutoChem 2920*) in 50 cm^3 min^{-1} of 10 % of H_2 in Ar. The metal surface and the size of the metallic crystallite of the catalysts with CZA metallic function have been determined by chemisorption using N_2O pulses at 60 °C in He atmosphere in a *Micromeritics AutoChem 2920* coupled to a *Balzers Instruments Omnistar* mass spectrometer through a thermostated line in order to analyze the amounts both of N_2 formed and of unreacted N_2O (according to the reaction: $N_2O+2Cu \rightarrow Cu_2O+N_2$) by monitoring the signals corresponding to masses 28 and 44, respectively. Based on the reacted gas volume, the active Cu surface was calculated, considering the adsorbate surface area (1.63×10^{19} at Cu/m^2). As both Cu and Fe react with N_2O, the metallic properties of Cu particles in the catalysts with $CuFe_2O_4$ spinel were determined by CO chemisorptions in the same *Micromeritics AutoChem 2920* equipment. Total acidity and acid strength distribution were measured by calorimetric measurements

of the differential adsorption of ammonia and subsequent temperature programmed desorption (TPD) of NH_3 in a Setaram TG-DSC 111 calorimeter connected on-line to a *Balzers Omnistar* mass spectrometer. The X-ray diffraction (XRD) analyses were measured on a *Bruker D8 Advance* diffractrometer with a CuKα1 radiation. The device is equipped with a Germanium primary monochromator, *Bragg-Brentano* geometry and with a CuKα1 wavelength of 1.5406 Å, corresponding to an X-ray tube with Cu anticathode. *Sol-X* dispersive energy detector was employed, with a window optimized for CuKα1 for limiting the fluorescence radiation. Data collection was carried out continuously with step of 0.04° in 2θ and measurement time per step of 12 s.

Temperature programmed oxidation (TPO) measurements were employed to estimate the carbon amount deposited on the deactivated catalysts and on the partially and fully regenerated catalysts. The samples were oxidized in air, following a heating ramp of 5 °C min^{-1} from room temperature up to 700 °C. The equipment used was a *TA Instrument SDT 2960* thermobalance connected on-line to a mass spectrometer (*Balzers Instruments Thermostar*) via a thermostated line in order to monitor the signals corresponding to the combustion gases (masses 14, 18, 28 and 44 corresponding to N_2, H_2O, CO and CO_2, respectively). The coke combustion cannot be monitored by thermogravimetry, as the thermogravimetric signal corresponding to coke combustion is masked with that of Cu oxidation, which occurs in parallel with coke combustion.

2.3. Experimental device and product analysis

The kinetic runs were carried out in an automated reaction equipment (*Microactivity Reference* from PID Eng & Tech) previously described elsewhere [36]. It is provided with an stainless steel isothermal fluidized-bed reactor (22 mm of internal diameter and total length of 460 mm) connected on-line to a gas chromatograph (*Agilent Micro GC 3000*) for product analysis. The fluidized bed reactor ensures isothermicity of the bed during the step of coke combustion with air.

The particle size of the catalyst (obtained by sieving) was 90-250 μm and an inert solid (carborundum, CSi, with 30-50 μm particle size) was also used in the reactor, in a inert/catalyst mass ratio of 8/1 in order to improve the hydrodynamic properties of the catalytic bed. The particle sizes of both solids are suitable for the bed hydrodynamics and for their separation after reaction, required for characterization.

The on-line analysis of the reforming products was carried out continuously (more representative and stable than discontinuous sampling). Accordingly, a small fraction of the reactor outlet stream is continuously diluted and carried by the auxiliary gas (a He stream of 30 cm^3 min^{-1}) to the gas chromatograph through a thermostated line (at 150 ºC) to avoid the condensation of liquid compounds. The gas chromatograph is provided with

four modules for the analysis of the following: (1) permanent gases (O_2, H_2, CO, and CH_4) with 5A molecular sieve capillary column; (2) light oxygenates (C_{2-}), CO_2 and water, with Plot Q capillary column; (3) C_2-C_4 hydrocarbons, with alumina capillary column; (4) oxygenated compounds (C_{2+}) with Stabilwax type column.

The experiments were conducted in reaction-regeneration cycles in order to analyze the recovery of the reaction indices in the successive reaction steps. The operating conditions for the steam reforming reaction are the following: temperature, 275, 300 or 315 °C; total pressure, 1.2 bar; steam/DME/He molar ratio, 3/1/0.85; P_{DME}, 0.24 bar; space time, 0.13 $g_{catalyst}$ h (g_{DME})$^{-1}$ for catalysts with CZA metallic function, and 0.29 $g_{catalyst}$ h (g_{DME})$^{-1}$ for catalyst with $CuFe_2O_4$ metallic function. The space time for the experiments with $CuFe_2O_4$/HZ30 catalyst was double, due to its lower activity and in order to achieve conversion values similar to those obtained with CZA/HZ30. Before each reforming reaction step, the catalyst was reduced using 10 % H_2 in He at 300 °C for 2 h with a total flow rate of 100 cm^3 min^{-1}.

The regeneration, by coke combustion with air (150 cm^3 min^{-1} to assure a correct fluidodynamic of the fluidized bed), was carried out *'in situ'* between subsequent reaction steps, following a temperature ramp of 5 °C min^{-1} from the reaction temperature up to the regeneration temperature (315 ºC or 500 ºC), which is then maintained constant for 2 h.

2.4. Reaction indices

The catalytic performance in SRD was studied in terms of DME conversion and H_2 yield, defined as follows:

$$X_{DME} = \frac{F_{DME,0} - F_{DME}}{F_{DME,0}} \tag{6}$$

$$Y_{H_2} = \frac{F_{H2}}{6F_{DME,0}} \tag{7}$$

where $F_{DME,0}$ and F_{DME} are the molar flow rates of DME at the reactor inlet and outlet, respectively, F_{H2} is the molar flow of H_2 at the reactor outlet, evaluated from its molar fraction (determined from chromatographic results) and the total molar flow rate (determined by atomic balances for H, C and O).

Moreover, an additional reaction index is defined, i.e., methanol effective conversion in the second step of the SRD process.

$$X_{MeOH} = \frac{F_{MeOH,0} - F_{MeOH}}{F_{MeOH,0}} \tag{8}$$

where $F_{MeOH,0}$ is the methanol molar flow rate calculated from DME conversion (double the number of DME moles converted, according to DME hydrolysis stoichiometry). F_{MeOH} is the methanol molar flow rate at the reactor outlet, determined experimentally by chromatography.

The formation of light hydrocarbons (mainly ethylene and propylene) has been observed under certain operation conditions and with zeolite HZ30 (without alkaline treatment) as acid function in the catalyst. The formation of these hydrocarbons has been quantified as their molar fraction in the product stream, x_{HCs}.

3. Results and Discussion

3.1. Properties of the fresh catalysts

The properties of the fresh catalysts are set out in Table 1. It is worth mentioning that the differences in the physical properties (BET surface area, pore volume and average pore size) between CZA/HZ30 and $CuFe_2O_4$/HZ30 catalysts are mainly due to differences in the metallic and acid function mass ratios of the bifunctional catalysts. According to the results in Table 1, the catalyst with HZ30 zeolite exhibits a higher BET surface area than that with the alkaline treated (AHZ30) acid function, although this treatment confers the zeolite a higher mesopore size and volume [14]. The acidity values prove that the alkaline treatment was effective for moderating the zeolite acidity, as CZA/AHZ30 shows less total acidity and weaker average acid strength than CZA/HZ30. Concerning the metallic properties, CZA based catalysts show better dispersion values with higher metallic surface values and smaller metallic particle size than the copper-ferrite spinel.

Table1

The TPR profiles of the $CuFe_2O_4$ metallic function and of the corresponding bifunctional catalyst are shown in Fig. 1. $CuFe_2O_4$ metallic function shows two reduction domains: the first one in the 230-360 ºC range corresponds to the reduction of $CuFe_2O_4$ to Cu and Fe_2O_3 and the subsequent reduction of Fe_2O_3 to Fe_3O_4, whereas the second domain in the 360-570 ºC range comprises Fe_3O_4 reduction to FeO followed by FeO reduction to Fe [29]. The TPR profile of the CZA metallic function and of the CZA/HZ30 catalyst have been reported elsewhere [14,37]. CZA metallic function exhibits a unique peak at around 190 ºC that corresponds to CuO reduction [14, 42]. The addition of the acid function to CZA or $CuFe_2O_4$ does not have a significant influence on the reducibility of the catalysts and, therefore, the TPR profiles of the bifunctional catalysts are similar to those of the corresponding metallic function [14,37].

Fig. 1

The XRD of the bifunctional $CuFe_2O_4$/HZ30 catalyst is shown in Fig. 2, in which the peaks corresponding to Cu-Fe spinel ($CuFe_2O_4$) confirm its formation in the synthesis process carried out in the laboratory. Besides, these results confirm that all the Cu in the $CuFe_2O_4$/HZ30 catalyst constitutes spinel $CuFe_2O_4$, given that other Cu species are not identified. Diffraction curves for the catalysts based on CZA metallic function have previously been reported [14,37] and show the peaks corresponding to CuO, ZnO and HZSM-5 phases separately. The main difference between them lied on the existence of $Cu_2Zn_4Al_2(OH)_{16}CO_34H_2O$ species in the catalyst with the alkali treated acid function (CZA/AHZ30).

Fig. 2

3.2. Reaction cycles followed by combustion of the coke deposited on the metallic function (at 315 ºC)

3.2.1. Catalysts with $CuZnOAl_2O_3$ metallic function

Coke combustion at 315 ºC has been studied since this is considered the maximum temperature allowed for avoiding Cu sintering in catalysts with $CuZnOAl_2O_3$ metallic function. Fig. 3 shows TPO profiles for CZA/AHZ30 deactivated after 20 h time on stream (black) and regenerated by coke combustion at 315 ºC for 2 h (blue). The TPO profile of the coke deposited on the deactivated catalyst shows two main peaks at 250 ºC and 410 ºC. The position of combustion peaks in supported metal catalysts and bi-functional catalysts is related to the proximity between the metal and the coke and to the metal ability to activate coke combustion. Consequently, the first peak is related to the coke deposited on the metal sites and the second peak is related to the coke deposited on the acid sites [43,44]. The mechanism of coke formation occurs presumably through methoxy ion intermediates [43], as proposed by Agarwal et al. for methanol steam reforming [45].

After coke combustion at 315 ºC, the TPO curve only shows the peak at the highest temperature, which corresponds to the coke deposited on the acid sites of the HZSM-5 zeolite, which evidences that coke combustion at 315 ºC is effective for the regeneration of the metallic function but it is not enough for regenerating the acid function. Moreover, it has been proven that there is no metal sintering after the regeneration at 315 ºC, as copper metal surface values of 56, 35 and 56 m^2/g_{Cu} have been measured for the fresh, deactivated and regenerated catalyst, respectively. However, Cu sintering is significant above this temperature as shown later.

Fig. 3

Fig. 4 shows the evolution with time on stream of DME conversion (graph a), MeOH effective conversion (graph b), and H_2 yield (graph c) for CZA/AHZ30 catalyst in the first and second reaction steps, with intermediate regeneration by combustion in air at 315 ºC. The reforming conditions were: 275 ºC; total pressure, 1.2 bar; P_{DME}, 0.24 bar; space-time, 0.13 $g_{catalyst}$ h $(g_{DME})^{-1}$; steam/DME molar ratio, 3.

After coke combustion, the activity for the SRM is recovered at zero time on stream as a consequence of the regeneration of the metallic function (Fig. 4), thus reaching a conversion value of 93 % (Fig. 4b). Nevertheless, the values at zero time of DME conversion (Fig. 4a) and H_2 yield (Fig. 4c) are lower than those obtained in the first reaction (fresh catalyst) (from 44 % to 40 %, and 43 % to 39 %, for X_{DME} and Y_{H2}, respectively). These results are explained because the coke deposited on the zeolite (responsible for DME hydrolysis) is not burned at 315 ºC, as observed in the TPO profile (Fig. 3). On the other hand, the evolution with time on stream of the DME and MeOH conversions and H_2 yield of the partially regenerated catalyst are similar to those obtained with the fresh catalyst. It should be noted that CH_4 has not been detected under any operating condition studied and CO formation is low (< 4 mol %) in all cases, especially with $CuFe_2O_4$/HZ30 catalyst (results shown in the following section).

Fig. 4

In order to study the behaviour of the CZA based catalysts with a higher coke content, another run under reaction-regeneration cycles was performed with CZA/HZ30 catalyst prepared with the pure HZSM-5 zeolite (with higher acid strength) and under reaction conditions that assure a high coke deactivation level. Fig. 5 shows the evolution with time on stream of DME conversion (graph a), effective MeOH conversion (graph b), H_2 yield (graph c) and hydrocarbons molar fraction (graph d) in three successive reaction steps at 315 °C. The regeneration was also carried out at 315 °C in air after each reaction step. It is worth mentioning that under these operating conditions a significant formation of hydrocarbons takes place by means of MeOH and DME transformation, which increases with time on stream (Fig. 5d).

Fig. 5

It is observed that MeOH conversion at zero time on stream is recovered for the three reaction cycles, whereas the initial values of DME conversion and H_2 yield progressively decrease for the second and third reactions. These results are qualitatively similar to those afore mentioned under lower coke deposition conditions (Fig. 4) and they are justified by the complete elimination at 315 ºC of the coke deposited on the metallic function, whereas the acid function does not recover its initial activity for the DME hydrolysis because the

coke deposited on the acid function is not removed, and consequently, the activity for DME hydrolysis progressively decreases in subsequent reactions.

It should be noted that the presence of coke remaining in the acid function enhances the formation of hydrocarbons, thereby, on the one hand, reducing the yield of H_2 and on the other hand, promoting coke formation [14]. The relationship between the results of hydrocarbon formation (Fig. 5d) and coke deposition are explained according to the hydrocarbon pool mechanism for hydrocarbons formation from MeOH/DME [46-50] and to the role of the intermediate organic species (such as polymethylbenzenes) in this mechanism [51-53]. The presence of coke components in the HZSM-5 zeolite (since they are not removed in the combustion) favours the formation of hydrocarbons when the catalyst is reused. Consequently, Fig. 5d shows that the induction period for the formation of hydrocarbons is shorter when the catalyst is reutilized in the second reaction. In the third reaction, the formation of hydrocarbon is attenuated as a consequence of the high coke deposition on the zeolite (accumulated in the successive reaction steps). This coke deposition deactivates the catalyst for hydrocarbon formation, and consequently this formation goes through a maximum.

The TPO profiles for the deactivated catalyst after the first and the third reactions (with coke combustion at 315 ºC between reactions (Fig. 6)) confirm the above mentioned results under low coke deposition conditions. On the one hand, it is observed that the first peak (with its maximum at 240 ºC) is just slightly higher for the reutilized catalyst, which indicates that the coke deposited on the metallic sites is totally eliminated by combustion at 315 °C, but it increases slightly after each successive reaction because deactivation is progressively more significant. On the other hand, the coke deposited on the zeolite (peak at 350-390 ºC) is considerably higher after the third reaction, as a consequence of coke accumulation in the successive partial combustions. Besides, it has been proven that there is no significant metal sintering, as the specific metal surface values for fresh, deactivated and regenerated catalyst are 55, 40 and 55 m^2/g_{Cu}, respectively.

Fig. 6

3.2.2. Catalysts with $CuFe_2O_4$ spinel metallic function

Fig. 7 shows the TPO profiles for the coke deposited on the deactivated $CuFe_2O_4$/HZ30 catalyst under given operating conditions (black), and after regeneration by coke combustion at 315 ºC (blue). The wide TPO profile for the deactivated catalyst can be deconvoluted into two peaks; the first peak corresponds to the coke deposited on the metallic spinel and the main peak at higher temperature corresponds to the coke deposited on the acid function. It is noteworthy that the second peak overlaps the first one (the shoulder in Fig. 7), which exhibits a higher combustion temperature than that

corresponding to the combustion of the coke deposited on the CZA metallic function (Figs. 3 and 6). The position of the main peak at high temperature is consistent with that shown in Fig. 3, since it corresponds to the coke deposited on the HZSM-5 zeolite. Moreover, the whole coke content deposited on this catalyst (4.1 wt%, total area under the TPO curve) is considerably higher than that shown in Figs. 3 and 6, since each reaction step at 300 ºC was followed by an additional reforming period at 500 ºC for 2 h (not showed in Fig. 8) in order to accelerate catalyst deactivation.

Fig. 7

The TPO profile of the catalyst after coke combustion at 315 ºC (blue line) exhibits a unique peak that corresponds to the coke deposited on the zeolite, which corroborates the complete elimination of the coke deposited on the metallic function. This result is qualitatively similar to that obtained for the CZA based catalyst (Fig. 3).

Fig. 8 shows the evolution with time on stream of DME conversion (graph a), effective conversion of MeOH (graph b) and yield of H_2 (graph c) in three successive reactions steps at 300 ºC, with intermediate regeneration steps consisting of coke combustion with air at 315 ºC. The results corresponding to the subsequent 2 h time on stream at 500 ºC in each reaction step, in order to accelerate catalyst deactivation, are not shown.

Fig. 8

DME conversion at zero time on stream decreases in the successive reactions from 0.56 for the fresh catalyst down to 0.4 for the twice reutilized catalyst (Fig. 8a). It is noteworthy that DME conversion at zero time on stream for the second and third reactions is even lower than that corresponding to 4 h time on stream in the preceding reaction, which is explained by the deactivation of the catalyst after the reforming period at 500 ºC for 2 h (results not shown in Fig. 8) in each reaction step. Nevertheless, it should be emphasized that MeOH conversion at zero time on stream slightly increases after successive reactions (Fig. 8b). As a consequence of both synergic and opposite effects, the H_2 yield at zero time on stream slightly decreases in the successive catalyst reutilizations (Fig. 8c). The activation of the $CuFe_2O_4$ metallic function after the coke combustion was also observed by Shimoda et al. [30, 54, 55], who explain it by redispersion of Cu via re-construction of Cu-Fe spinel. As shown in Fig. 8b, the activating effect of the spinel progressively decreases in the subsequent regeneration steps.

The afore-mentioned results of reaction-regeneration cycles for CZA and $CuFe_2O_4$ based bifunctional catalysts with different level of coke deposition highlight that coke combustion at 315 ºC is enough for the regeneration of the metallic function but not for the

regeneration of the HZSM-5 zeolite. The remaining coke provokes a progressive loss of catalyst activity for DME hydrolysis (Eq 1) in the successive cycles, and consequently, a lower H_2 yield. Therefore, a higher regeneration temperature is required to remove all the coke deposited on the zeolite after consecutive reactions. According to the peak positions in the TPO profiles corresponding to the coke deposited on the zeolite (Fig. 3, 6 and 7), a temperature around 500 ºC is required for total removal of coke in a short period of time. This temperature is appropriate for the regeneration of HZSM-5 zeolites used in different processes, which are regenerated at the 500-570 ºC temperature range, this last temperature being limited by the hydrothermal stability of the zeolites [56-58].

3.3. Reaction cycles followed by combustion of the coke deposited on both the metallic and acid functions (at 500 ºC)

3.3.1. Catalysts with $CuZnOAl_2O_3$ metallic function

Fig. 9 shows the evolution with time on stream of DME conversion (graph a), MeOH effective conversion (graph b) and H_2 yield (graph c) for CZA/AHZ30 catalyst in three successive reaction cycles at 300 °C, with intermediate regeneration in air at 500 °C for assuring the complete combustion of the coke deposited (both on metallic and acid sites). The reaction indices remain almost constant along each reaction step due to the short duration of the runs (3 h) and the high stability of the catalyst (the acid strength of HZSM-5 zeolite is attenuated by alkaline treatment), which minimizes the hydrocarbon formation and coke deposition [14]. The TPO results of the deactivated catalyst are not shown since the coke content measured is almost negligible. Furthermore, it should be noted that DME conversion is higher than the corresponding to Fig. 4 (for the same catalyst), since the higher reaction temperature (300 ºC in Fig. 9 and 275 ºC in Fig. 4) notably favors the reaction rate for DME hydrolysis on the acid function.

Fig. 9

Fig. 9 shows that MeOH conversion and H_2 yield at zero time on stream undergo a continuous and accumulative decrease when the catalyst is reused, while DME conversion suffers a slight decrease in the subsequent reactions, from 0.54 to 0.51. This irreversible catalyst activity loss is caused by sintering of the metallic function during the coke combustion steps with air at 500 ºC, which affects the MeOH reforming step, and consequently, the displacement of DME hydrolysis equilibrium is not favored.

The chemisorptions by N_2O pulses confirms the sintering of Cu particles for the catalysts subjected to two regeneration steps at 500 ºC, with an specific metallic surface of 45

m^2/g_{Cu}, which is considerably smaller than that corresponding to the fresh catalyst (56 m^2/g_{Cu}).

Considering the difficulty for fully recovering the catalyst activity, a thermal treatment up to 500 ºC might be appropriate to equilibrate the catalyst with CZA metallic function, so that the metallic function gains in stability, but at the expense of activity loss. Therefore, the optimization of the composition for the bifunctional catalyst would be required, because a higher metallic/acid functions ratio would be needed as the metal function becomes less active [30].

3.3.2. Catalyst with $CuFe_2O_4$ metallic function

Fig. 10 shows the evolution with time on stream of DME conversion (graph a), MeOH effective conversion (graph b) and H_2 yield (graph c) for three subsequent reaction steps. The operating conditions are those used in Fig. 8, and as in that case, each reaction step was followed by an additional reforming period at 500 ºC for 2 h (not showed in Fig. 10) in order to accelerate coke deposition. The regeneration between reaction steps has been conducted at 500 °C by combustion with air. After this combustion at 500 ºC it is observed that the coke deposited on the catalyst has been fully removed (plain profile of TPO curve for the regenerated catalyst, not shown).

Fig. 10

An increase is observed in the values at zero time on stream of MeOH conversion (from 0.90 to 0.93) (Fig. 10a), DME conversion (from 0.56 to 0.72) (Fig. 10b) and H_2 yield (from 0.52 to 0.66) (Fig. 10c) after the successive regeneration steps, due to the total removal of the coke deposited on both the metallic and acid functions and as well as Cu redispersion within the spinel matrix. The increase in MeOH conversion after regeneration at 500 ºC corroborates the results previously obtained after regeneration at 315 ºC (shown in Fig. 8). Cu metallic surface areas for the fresh and the once regenerated catalyst are 5.9 and 8.4 m^2/g_{Cu}, respectively, which confirm a considerable redispersion of the Cu within the spinel matrix. After the second regeneration step, the increase in the Cu metallic surface is lower, 8.9 m^2/g_{Cu}, thus indicating that after successive regenerations the catalyst attains an equilibrium state.

It is noteworthy that the advantage of increasing the catalyst activity after regeneration may be a drawback for the industrial implantation of the process, since it hinders the design and control of the reactor and of the units for separation and purification of the product stream. According to the results, an equilibration treatment for the catalyst would be appropriate in order to avoid this drawback. The equilibration treatment would require a

reaction-regeneration step under reaction conditions that assure accelerated coke deposition. It has been proven that the catalyst equilibration is not achieved by a thermal treatment of the fresh catalyst at 500 ºC, since spinel activation by Cu redispersion is only achieved by removing the coke deposited on the metallic sites of the catalyst.

4. Conclusions

The bifunctional catalysts prepared with CZA or $CuFe_2O_4$ spinel metallic functions and HZSM-5 zeolite (pure or alkali treated) acid function have a notably different behavior when used in the steam reforming of DME under reaction-regeneration cycles. This different behavior is due to the high temperature (500 ºC) required for the combustion of the coke deposited on the zeolite and to the effect this combustion has on the activity of the metallic function. In both catalysts the coke is deposited on both the metallic and the acid functions; the coke deposited on the metallic function is completely removed by combustion with air at 315 ºC, while the total removal of coke from the zeolite must be carried out at 500 ºC. At this temperature, CZA metallic function undergoes Cu sintering, which poses a problem for industrial implementation. Thus, Cu sintering has a considerable attenuating effect on methanol reforming reaction and, consequently H_2 yield progressively decreases at the beginning of each subsequent reaction step.

Nevertheless, the regeneration by combustion with air at 500 ºC does not involve Cu sintering in the $CuFe_2O_4$ spinel, but increases its activity after the regeneration step. This reactivation step of the spinel is attributable to a Cu redispersion within the spinel matrix and it is progressively attenuated in the successive regeneration steps.

According to the results obtained, $CuFe_2O_4$/HZSM-5 is an adequate catalyst for operating under reaction-regeneration cycles in the SRD reaction. A previous deactivation-regeneration cycle, under high coke deposition conditions in the deactivation step, is necessary in order to attain a constant behaviour of the catalyst.

Nomenclature

d_M — average diameter of Ni metal particle, nm

d_{pore} — pore diameter, Å

$F_{DME}, F_{DME,0}$ — molar flow rate of dimethyl ether (DME) at the reactor outlet and in the feed, respectively

$F_{MeOH}, F_{MeOH,0}$ — molar flow rate of methanol at the reactor outlet and estimated by DME conversion, respectively

F_{H2} — molar flow rate of H_2 at the reactor outlet, mol/min

P_{DME} — DME partial pressure, bar

S_{BET} — BET surface area, $m^2\,g^{-1}$

$S_{metallic}$ — specific metal surface area, $m^2\,g_{metal}^{-1}$

$V_{mesopore}, V_{micropore}$ — mesopore and micropore volume, $cm^3\,g^{-1}$

X_{DME}, X_{MeOH} — DME conversion and methanol effective conversion in the second step of the SRD process, respectively

x_{HCs} — molar fraction of hydrocarbons

Y_{H2} — yield of H_2, %

References

[1] A. Qi, B. Peppley, K. Karanet, Integrated fuel processors for fuel cell application: A review, Fuel Process. Technol. 88 (2007) 3-22.

[2] H. Balat, E. Kirtay, Hydrogen from biomass-Present scenario and future prospects, Int. J. Hydrogen Energy 35 (2010) 7416-7426.

[3] T.A. Semelsberger, R.L. Borup, H.L. Greene, Dimethyl ether (DME) as an alternative fuel, J. Power Sources 156 (2006) 497-511.

[4] C. Arcoumanis, C. Bae, R. Crookes, E. Kinoshita, The potential of dimethyl ether (DME) as an alternative fuel for compression-ignition engines: A review, Fuel 87 (2008) 1014-1030.

[5] Y. Tanaka, R. Kikuchi, T. Takeguchi, K. Eguchi, Steam reforming of dimethyl ether over composite catalysts of γ-Al_2O_3 and Cu-based spinel, Appl. Catal. B-Environ. 57 (2005) 211-222.

[6] T.A. Semelsberger, K.C. Ott, R.L. Borup, H.L. Greene, Generating hydrogen-rich fuel-cell feeds from dimethyl ether (DME) using physical mixtures of a commercial $Cu/Zn/Al_2O_3$ catalyst and several solid-acid catalysts, Appl. Catal. B-Environ. 65 (2006) 291-300.

[7] Y. Yamada, T. Mathew, A. Ueda, H. Shioyama, T. Kobayashi, A novel DME steam-reforming catalyst designed with fact database on-demand, Appl. Surf. Sci. 252 (2006) 2593-2597.

[8] Q. Zhang, J. Xu, F. Fan, D. Sun, G. Xu, S. Zhang, Z. Zhu. Application of porous anodic alumina monolith catalyst in steam reforming of dimethyl ether: Cu/γ-Al_2O_3/Al catalyst degradation behaviors and catalytic activity improvement by pre-competition impregnation method, Fuel Process. Technol. 119 (2014) 52-59.

[9] M. Higo, K. Dowaki, A Life Cycle Analysis on a Bio-DME Production System considering the Species of Biomass Feedstock in Japan and Papua New Guinea, Appl. Energy 87 (2010) 58-67.

[10] A.T. Aguayo, J. Ereña, I. Sierra, M. Olazar, J. Bilbao, Deactivation and regeneration of hybrid catalysts in the single-step synthesis of dimethyl ether from syngas and CO_2, Catal. Today 106 (2005) 265-70.

[11] D.A. Bulushev, J.R.H. Ross, Catalysis for Conversion of Biomass to Fuels via Pyrolysis and Gasification: A Review, Catal. Today 171 (2011) 1-13.

[12] G.A. Olah, A. Goeppert, G.K.S. Prakash, Chemical recycling of carbon dioxide to methanol and dimethyl ether: From greenhouse gas to renewable, environmentally carbon neutral fuels and synthetic hydrocarbons, J. Org. Chem. 74 (2009) 487-498.

[13] T.A. Semelsberger, K.C. Ott, R.L. Borup, H.L. Greene, Role of the acidity on the hydrolysis of dimethyl ether to methanol, Appl. Catal. A-Gen. 61 (2005) 281-287.

[14] J. Vicente, A.G. Gayubo, J. Ereña, A.T. Aguayo, M. Olazar, J. Bilbao, Improving the DME steam reforming catalyst by alkaline treatment of the HZSM-5 zeolite, Appl. Catal. B-Environ. 130-131 (2013) 73-83.

[15] T. Kawabata, H. Matsuoka, T. Shisido, D. Li, Y. Tian, T. Sano, K. Takehira, Steam reforming of dimethyl ether over ZSM-5 coupled with $Cu/ZnO/Al_2O_3$ catalyst prepared by homogeneous precipitation, Appl. Catal. A-Gen. 308 (2006) 82-90.

[16] K. Takeishi, H. Suzuki, Steam reforming of dimethyl ether, Appl. Catal. A-Gen. 260 (2004) 111-117.

[17] K. Faungnawakij, Y. Tanaka, N. Shimoda, T. Fukunaga, R. Kikuchi, K. Eguchi, Hydrogen production from dimethyl ether steam reforming over composite catalysts of copper ferrite spinel and alumina, Appl. Catal. B-Environ. 74 (2007) 144-151.

[18] K. Faungnawakij, N. Shimoda, T. Fukunaga, R. Kikuchi, K. Eguchi, Cu-based spinel catalysts CuB_2O_4 (B= Fe, Mn, Cr, Ga, Al, Fe0.75Mn0.25) for steam reforming of dimethyl ether, Appl. Catal. A-Gen. 341 (2008) 139-145.

[19] K. Faungnawakij, T. Fukunaga, R. Kikuchi, K. Eguchi, Deactivation and regeneration behaviors of copper spinel-alumina composite catalysts in steam reforming of dimethyl ether, J. Catal. 256 (2008) 37-44.

[20] K. Faungnawakij, N. Shimoda, N. Viriya-Empikul, R. Kikuchi, K. Eguchi, Limiting mechanisms in catalytic steam reforming of dimethyl ether, Appl. Catal. B-Environ. 97 (2010) 21-27.

[21] X. Wang, X. Pan, R. Lin, S. Kou, W. Zou, J.X. Ma, Steam reforming of dimethyl ether over Cu-Ni/γ-Al_2O_3 bi-functional catalyst prepared by deposition-precipitation method, Int. J. Hydrogen Energy 35 (2010) 4060-4068.

[22] T.A. Semelsberger, K.C. Ott, R.L. Borup, H.L. Greene, Generating hydrogen-rich fuel-cell feeds from dimethyl ether using Cu/Zn supported on various solid-acid substrates, Appl. Catal. A-Gen. 309 (2006) 210-223.

[23] S.D. Badmaev, G.G. Volkova, V.D. Belyaev, V.A. Sobyanin, Steam reforming of dimethyl ether to hydrogen-rich gas, Reac. Kinet. Catal. Lett. 90 (2007) 205-211.

[24] D. Feng, Y. Zuo, D. Wang, J. Wang, Steam reforming of dimethyl ether over coupled ZSM-5 and Cu-Zn-based catalysts, Chinese J. Catal. 30 (2009) 223-229.

[25] T. Matsumoto, T. Nishiguchi, H. Kanai, K. Utani, Y. Matsumura, S. Imamura, Steam reforming of dimethyl ether over H-mordenite-Cu/CeO_2 catalysts, Appl. Catal. A-Gen. 276 (2004) 267-273.

[26] T. Nishiguchi, K. Oka, T. Matsumoto, H. Kanai, K. Utani, S. Imamura, Durability of WO_3/ZrO_2-CuO/CeO_2 catalysts for steam reforming of dimethyl ether, Appl. Catal. A-Gen. 301 (2006) 66-74.

[27] K. Oka, T. Nishiguchi, H. Kanai, K. Utani, S. Imamura, Active state of tungsten oxides on WO_3/ZrO_2 catalyst for steam reforming of dimethyl ether combined with CuO/CeO_2, Appl. Catal. A-Gen. 309 (2006) 187-191.

[28] N. Shimoda, K. Faungnawakij, R. Kikuchi, T. Fukunaga, K. Eguchi, Catalytic performance enhancement by heat treatment of $CuFe_2O_4$ spinel and γ-alumina composite catalysts for steam reforming of dimethyl ether, Appl. Catal. A-Gen. 365 (2009) 71-78.

[29] N. Shimoda, K. Faungnawakij, R. Kikuchi, K. Eguchi, Degradation and regeneration of copper-iron spinel and zeolite composite catalysts in steam reforming of dimethyl ether, Appl. Catal. A-Gen. 378 (2010) 234-242.

[30] N. Shimoda, K. Faungnawakij, R. Kikuchi, K. Eguchi, A study of various zeolites and $CuFe_2O_4$ spinel composite catalysts in steam reforming and hydrolysis of dimethyl ether, Int. J. Hydrogen Energy 36 (2011) 1433-1441.

[31] K. Faungnawakij, N. Shimoda, T. Fukunaga, R. Kikuchi, K. Eguchi, Crystal structure and surface species of $CuFe_2O_4$ spinel catalysts in steam reforming of dimethyl ether, Appl. Catal. B-Environ. 92 (2009) 341-350.

[32] S. Kameoka, T. Tanabe, A. Pamg Tsai, Self-assembled porous nano-composite with high catalytic performance by reduction of tetragonal spinel $CuFe_2O_4$, Appl. Catal. A-Gen. 375 (2010) 163-171.

[33] S. Sá, J.M. Sousa, A. Mendes, Steam reforming of methanol over a $CuO/ZnO/Al_2O_3$ catalyst, part I: Kinetic modeling, Chem. Eng. Sci. 66 (2011) 4913-4921.

[34] D.R. Palo, R.A. Dagle, J.D. Holladay, Methanol Steam Reforming for Hydrogen Production, Chem. Rev. 107 (2007) 3992–4021.

[35] T. Fukunaga, N. Ryumon, S. Shimazu, The influence of metals and acidic oxide species on the steam reforming of dimethyl ether (DME), Appl. Catal. A-Gen. 348 (2008) 193-200.

[36] J. Ereña, J. Vicente, A.T. Aguayo, A.G. Gayubo, M. Olazar, J. Bilbao, Effect of combining metallic and acid functions in CZA/HZSM-5 desilicated zeolite catalysts on the DME steam reforming in a fluidized bed, Int. J. Hydrogen Energy 38 (2013) 10019-10029.

[37] J. Ereña, J. Vicente, A.T. Aguayo, M. Olazar, J. Bilbao, A.G. Gayubo, Kinetic behaviour of catalysts with different $CuO-ZnO-Al_2O_3$ metallic function compositions in DME steam reforming in a fluidized bed, Appl. Catal. B-Environ. 142-143 (2013) 315-322.

[38] J.P. Shen, C. Song, Influence of preparation method on performance of Cu/Zn-based catalysts for low-temperature steam reforming and oxidative steam reforming of methanol for H_2 production for fuel cells, Catal. Today 77 (2002) 89-98.

[39] Y. Kawamura, K. Yamamoto, N. Ogura, T. Katsumata, A. Igarashi, Preparation of $Cu/ZnO/Al_2O_3$ catalyst for a micro methanol reformer, J. Power Sources 150 (2005) 20-26.

[40] J. Ereña, J.M. Arandes, R. Garoña, A.G. Gayubo, J. Bilbao, Study of the preparation and composition of the metallic function for the selective hydrogenation of CO_2 to gasoline over bifunctional catalysts, J. Chem. Tech. Biotechnol. 78 (2003) 161-166.

[41] A.G. Gayubo, A. Alonso, B. Valle, A.T. Aguayo, J. Bilbao, Selective production of olefins from bioethanol on HZSM-5 zeolite catalysts treated with NaOH, Appl. Catal. B-Environ. 97 (2010) 299-306.

[42] J. Agrell, M. Boutonnet, I. Melián-Cabrera, J.L.G. Fierro, Production of hydrogen from methanol over binary Cu/ZnO catalysts: Part I. Catalyst preparation and characterization, Appl. Catal. A-Gen. 253 (2003) 201-211.

[43] J. Vicente, J. Ereña, L. Oar-Arteta, M. Olazar, J. Bilbao, A.G. Gayubo, Effect of Operating Conditions on Dimethyl Ether Steam Reforming in a Fluidized Bed Reactor with a $CuO–ZnO–Al_2O_3$ and Desilicated ZSM-5 Zeolite Bifunctional Catalyst, Ind. Eng. Chem. Res. 53 (2014) 3462-3471.

[44] J. Ereña, I. Sierra, M. Olazar, A.G. Gayubo, A.T. Aguayo, Deactivation of a $CuO−ZnO−Al_2O_3/γ-Al_2O_3$. Catalyst in the Synthesis of Dimethyl Ether, Ind. Eng. Chem. Res. 47 (2008) 2238–2247.

[45] V.Agarwal, S. Patel, K. K. Pant, H_2 production by steam reforming of methanol over Cu/ZnO/Al$_2$O$_3$ catalysts: transient deactivation kinetics modeling, Appl. Catal. A-Gen. 279 (2005) 155−164.

[46] I.M. Dahl, S. Kolboe, On the Reaction Mechanism for Hydrocarbon Formation from Methanol over SAPO-34: 2. Isotopic Labeling Studies of the Co-reaction of Propene and Methanol, J. Catal. 161 (1996) 304-309.

[47] A.T. Aguayo, A.G. Gayubo, R. Vivanco, A. Alonso, J. Bilbao, Initiation Step and Reactive Intermediates in the Transformation of Methanol into Olefins over SAPO-18 Catalyst, Ind. Eng. Chem. Res. 44 (2005) 7279-7286.

[48] U. Olsbye, M. Bjørgen, S. Svelle, K.P. Lillerud, S. Kolboe, Mechanistic insight into the methanol-to-hydrocarbons reaction, Catal. Today 106 (2005) 108-111.

[49] M. Bjørgen, S. Svelle, F. Joensen, J. Nerlov, S. Kolboe, F. Bonino, L. Palumbo, S. Bordiga, U. Olsbye, Conversion of methanol to hydrocarbons over zeolite H-ZSM-5: On the origin of the olefinic species, J. Catal. 249 (2007) 195-207.

[50] K. Hemelsoet, J. Van Der Mynsbrugge, K. De Wispelaere, M. Waroquier, V. Van Sepybroeck, Unraveling the reaction mechanisms governing methanol-to-olefins catalysis by theory and experiment, ChemPhysChem 14 (2013) 1526-1545.

[51] M. Guisnet, Coke molecules trapped in the micropores of zeolites as active species in hydrocarbon transformations, J. Mol. Catal. A: Chemical 182 (2002) 367-382.

[52] F.L. Bleken, K. Barbera, F. Bonino, U. Olsbye, K.P. Lillerud, S. Bordiga, P. Beato, T.V.W. Janssens, S. Svelle, Catalyst deactivation by coke formation in microporous and desilicated zeolite H-ZSM-5 during the conversion of methanol to hydrocarbons, J. Catal. 307 (2013) 62-73.

[53] T.V.W. Janssens, S. Svelle, U. Olsbye, Kinetic modeling of deactivation profiles in the methanol-to-hydrocarbons (MTH) reaction: A combined autocatalytic–hydrocarbon pool approach, J. Catal. 308 (2013) 122-130.

[54] N. Shimoda, H. Muroyama, T. Matsui, K. Faungnawakij, R. Kikuchi, K. Eguchi, Dimethyl ether steam reforming under daily start-up and shut-down (DSS)-like operation over CuFe$_2$O$_4$ spinel and alumina composite catalysts, Appl. Catal. A-Gen. 409-410 (2011) 91-98.

[55] K. Faungnawakij, K. Eguchi, Dimethyl Ether—Reforming Catalysts for Hydrogen Production, Catal. Surv. Asia 15 (2011) 12-24.

[56] A.G. Gayubo, A.T. Aguayo, M. Olazar, R. Vivanco, J. Bilbao, Kinetics of the irreversible deactivation on the HZSM-5 zeolite catalyst in the MTO Process, Chem. Eng. Sci. 58 (2003) 5239-5249.

[57] B. Valle, A.G. Gayubo, A. Alonso, A.T. Aguayo, J. Bilbao, Hydrothermally stable HZSM-5 zeolite catalysts for the transformation of crude bio-oil into hydrocarbons, Appl. Catal. B-Environ. 100 (2010) 318-327.

[58] A.T. Aguayo, A.G. Gayubo, A. Ateka, M. Gamero, M. Olazar, J. Bilbao, Joint transformation of methanol an n-butane into olefins on a HZSM-5 zeolite catalyst in reaction-regeneration cycles, Ind. Eng. Chem. Res. 51 (2012) 13073-13084.
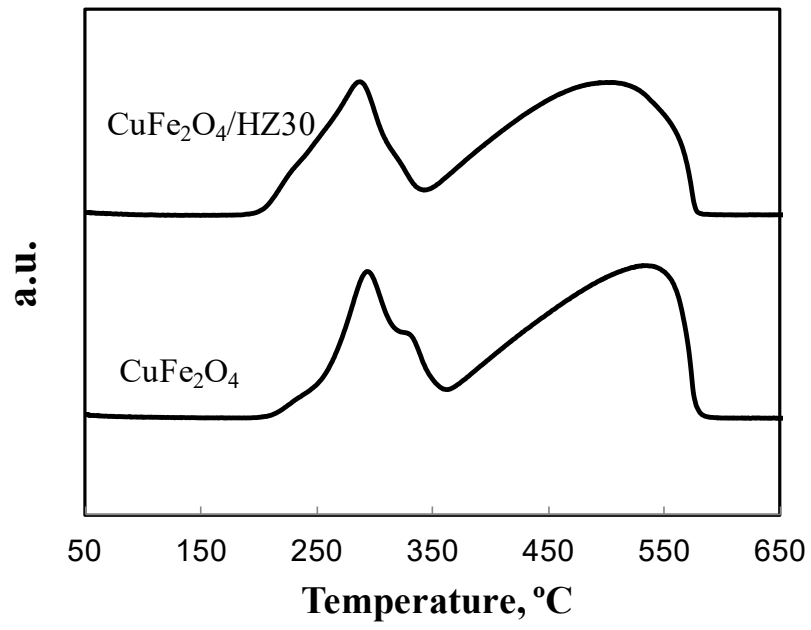
Figure captions

Fig. 1.   Temperature programmed reduction (TPR) profiles of the $CuFe_2O_4$ catalyst and $CuFe_2O_4$/HZ30 bifunctional catalyst.

Fig. 2.   XRD spectra of the $CuFe_2O_4$/HZ30 catalyst.

Fig. 3.   TPO profiles for CZA/AHZ30 catalyst deactivated (thick black line) and regenerated (thin blue line) in one reaction-regeneration cycle. Reaction conditions: 275 °C; 1.2 bar; P_{DME}, 0.24 bar; space-time, 0.13 $g_{catalyst}$ h $(g_{DME})^{-1}$; steam/DME molar ratio, 3; time on stream, 20 h. Regeneration with air at 315 °C for 2 h.

Fig. 4.   Evolution with time on stream of DME conversion (a), effective MeOH conversion (b), and H_2 yield (c), for CZA/AHZ30 catalyst used in two consecutive reaction-regeneration cycles. Reaction conditions: 275 °C; 1.2 bar; P_{DME}, 0.24 bar; space-time, 0.13 $g_{catalyst}$ h $(g_{DME})^{-1}$; steam/DME molar ratio, 3; Regeneration with air at 315 °C for 2 h.

Fig. 5.   Evolution with time on stream of DME conversion (a), effective MeOH conversion (b), H_2 yield (c) and HC-s molar fraction (d) for CZA/HZ30 catalyst used in three consecutive reaction-regeneration cycles. Reaction conditions: 315 °C; 1.2 bar; P_{DME}, 0.24 bar; space-time, 0.13 $g_{catalyst}$ h $(g_{DME})^{-1}$; steam/DME molar ratio, 3. Regeneration with air at 315 °C for 2 h.

Fig. 6.   TPO profiles for used CZA/HZ30 catalyst after the 1st and 3rd reaction step, with regeneration between reaction steps. Reaction conditions: 315 °C; 1.2 bar; P_{DME}, 0.24 bar; space-time, 0.13 $g_{catalyst}$ h $(g_{DME})^{-1}$; steam/DME molar ratio, 3. Regeneration with air at 315 °C for 2 h.

Fig. 7.   TPO profiles for $CuFe_2O_4$/HZ30 catalyst deactivated (thick black line) and regenerated (thin blue line) in the third reaction-regeneration cycle. Reaction conditions: 4 h at 300 °C (followed by 2h at 500 ºC, not shown), 1.2 bar; P_{DME}, 0.24 bar; space-time, 0.29 $g_{catalyst}$ h $(g_{DME})^{-1}$; steam/DME molar ratio, 3. Regeneration with air at 315 °C for 2 h.

Fig. 8.   Evolution with time on stream of DME conversion (a), effective MeOH conversion (b) and H_2 yield (c) for $CuFe_2O_4$/HZ30 catalyst in three consecutive reaction- regeneration cycles. Reaction conditions: 4 h at 300 °C (followed by 2 h at 500 ºC, not shown) 1.2 bar; P_{DME}, 0.24 bar; space-time, 0.29 $g_{catalyst}$ h $(g_{DME})^{-1}$; steam/DME molar ratio, 3. Regeneration with air at 315 °C for 2 h.

Fig. 9.   Evolution with time on stream of DME conversion (a), effective MeOH conversion (b) and H_2 yield (c) for CZA/AHZ30 catalyst in three consecutive reaction- regeneration cycles. Reaction conditions: 3 h at 300 °C; 1.2 bar; P_{DME}, 0.24 bar; space-time, 0.13 $g_{catalyst}$ h $(g_{DME})^{-1}$; steam/DME molar ratio, 4. Regeneration with air at 500 °C for 2 h.

Fig. 10.   Evolution with time on stream of DME conversion (a), effective MeOH conversion (b) and H_2 yield (c) for $CuFe_2O_4$/HZ30 catalyst in three consecutive reaction- regeneration cycles. Reaction conditions: 4 h at 300 °C (followed by 2h at 500 ºC, not shown); 1.2 bar; P_{DME}, 0.24 bar; space-time, 0.29 $g_{catalyst}$ h $(g_{DME})^{-1}$; steam/DME molar ratio, 3. Regeneration with air at 500 °C for 2 h.

Figure captions

Fig. 1. Temperature programmed reduction (TPR) profiles of the $CuFe_2O_4$ catalyst and $CuFe_2O_4$/HZ30 bifunctional catalyst.

Fig. 2. XRD spectra of the $CuFe_2O_4$/HZ30 catalyst.

Fig. 3. TPO profiles for CZA/AHZ30 catalyst deactivated (thick black line) and regenerated (thin blue line) in one reaction-regeneration cycle. Reaction conditions: 275 °C; 1.2 bar; P_{DME}, 0.24 bar; space-time, 0.13 $g_{catalyst}$ h $(g_{DME})^{-1}$; steam/DME molar ratio, 3; time on stream, 20 h. Regeneration with air at 315 °C for 2 h.

Fig. 4. Evolution with time on stream of DME conversion (a), effective MeOH conversion (b), and H_2 yield (c), for CZA/AHZ30 catalyst used in two consecutive reaction-regeneration cycles. Reaction conditions: 275 °C; 1.2 bar; P_{DME}, 0.24 bar; space-time, 0.13 $g_{catalyst}$ h $(g_{DME})^{-1}$; steam/DME molar ratio, 3; Regeneration with air at 315 °C for 2 h.

Fig. 5. Evolution with time on stream of DME conversion (a), effective MeOH conversion (b), H_2 yield (c) and HC-s molar fraction (d) for CZA/HZ30 catalyst used in three consecutive reaction-regeneration cycles. Reaction conditions: 315 °C; 1.2 bar; P_{DME}, 0.24 bar; space-time, 0.13 $g_{catalyst}$ h $(g_{DME})^{-1}$; steam/DME molar ratio, 3. Regeneration with air at 315 °C for 2 h.

Fig. 6. TPO profiles for used CZA/HZ30 catalyst after the 1st and 3rd reaction step, with regeneration between reaction steps. Reaction conditions: 315 °C; 1.2 bar; P_{DME}, 0.24 bar; space-time, 0.13 $g_{catalyst}$ h $(g_{DME})^{-1}$; steam/DME molar ratio, 3. Regeneration with air at 315 °C for 2 h.

Fig. 7. TPO profiles for $CuFe_2O_4$/HZ30 catalyst deactivated (thick black line) and regenerated (thin blue line) in the third reaction-regeneration cycle. Reaction conditions: 4 h at 300 °C (followed by 2h at 500 ºC, not shown), 1.2 bar; P_{DME}, 0.24 bar; space-time, 0.29 $g_{catalyst}$ h $(g_{DME})^{-1}$; steam/DME molar ratio, 3. Regeneration with air at 315 °C for 2 h.

Fig. 8. Evolution with time on stream of DME conversion (a), effective MeOH conversion (b) and H_2 yield (c) for $CuFe_2O_4$/HZ30 catalyst in three consecutive reaction- regeneration cycles. Reaction conditions: 4 h at 300 °C (followed by 2 h at 500 ºC, not shown) 1.2 bar; P_{DME}, 0.24 bar; space-time, 0.29 $g_{catalyst}$ h $(g_{DME})^{-1}$; steam/DME molar ratio, 3. Regeneration with air at 315 °C for 2 h.

Fig. 9. Evolution with time on stream of DME conversion (a), effective MeOH conversion (b) and H_2 yield (c) for CZA/AHZ30 catalyst in three consecutive reaction- regeneration cycles. Reaction conditions: 3 h at 300 °C; 1.2 bar; P_{DME}, 0.24 bar; space-time, 0.13 $g_{catalyst}$ h $(g_{DME})^{-1}$; steam/DME molar ratio, 4. Regeneration with air at 500 °C for 2 h.

Fig. 10. Evolution with time on stream of DME conversion (a), effective MeOH conversion (b) and H_2 yield (c) for $CuFe_2O_4$/HZ30 catalyst in three consecutive reaction- regeneration cycles. Reaction conditions: 4 h at 300 °C (followed by 2h at 500 ºC, not shown); 1.2 bar; P_{DME}, 0.24 bar; space-time, 0.29 $g_{catalyst}$ h $(g_{DME})^{-1}$; steam/DME molar ratio, 3. Regeneration with air at 500 °C for 2 h.

FIGURES

Figure 1
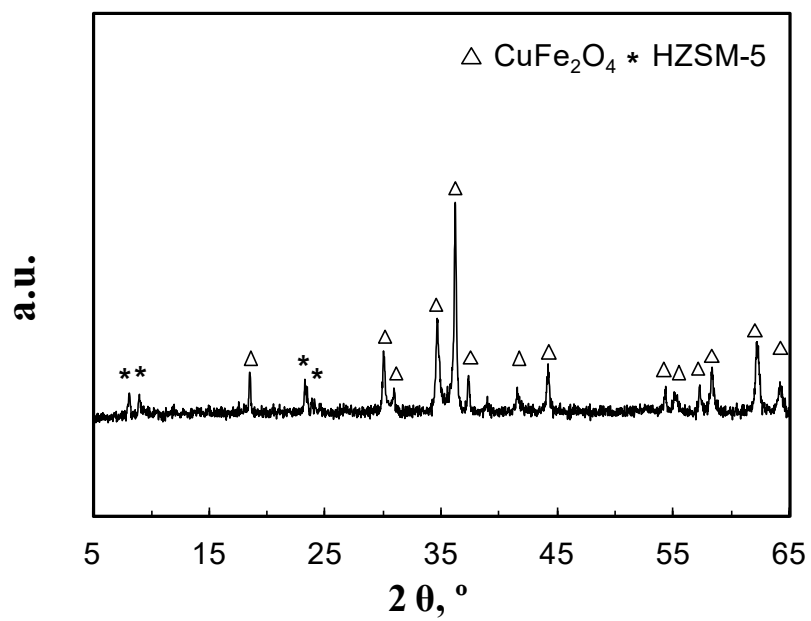
Figure 2
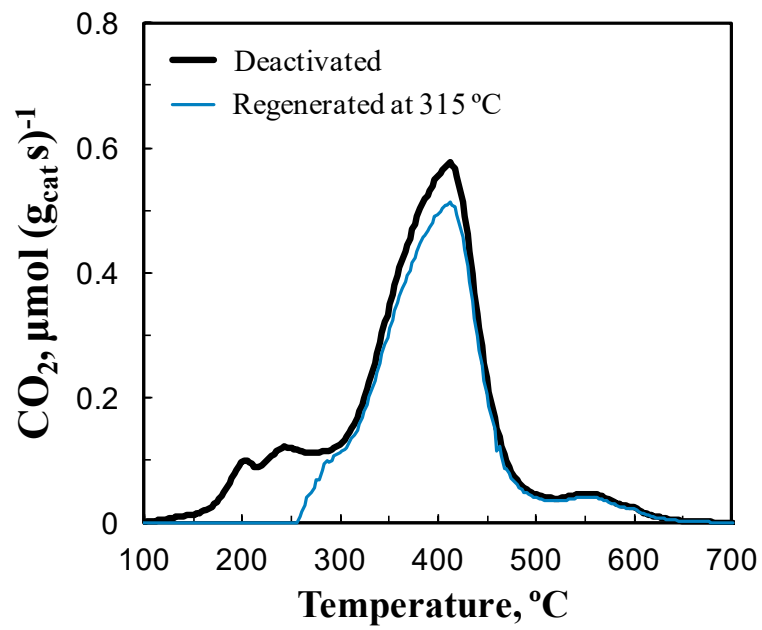
Figure 3
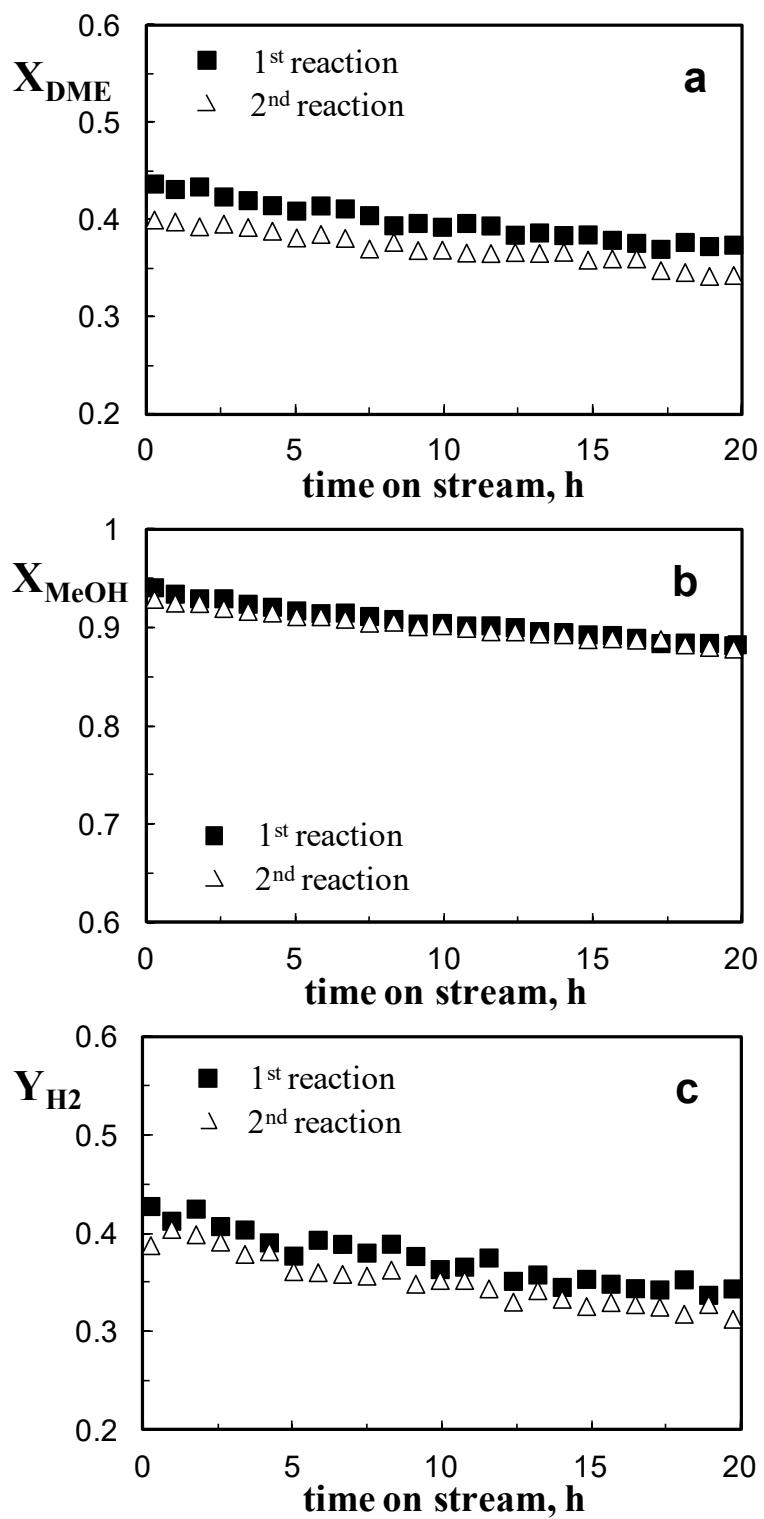
Figure 4
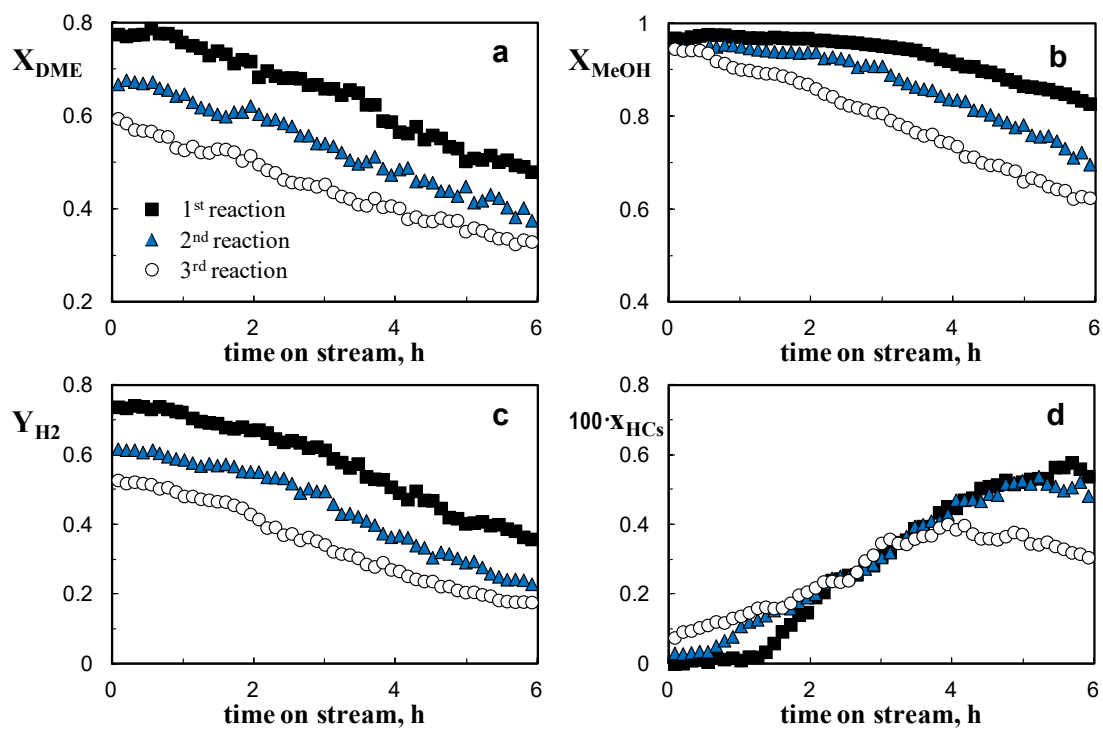
Figure 5
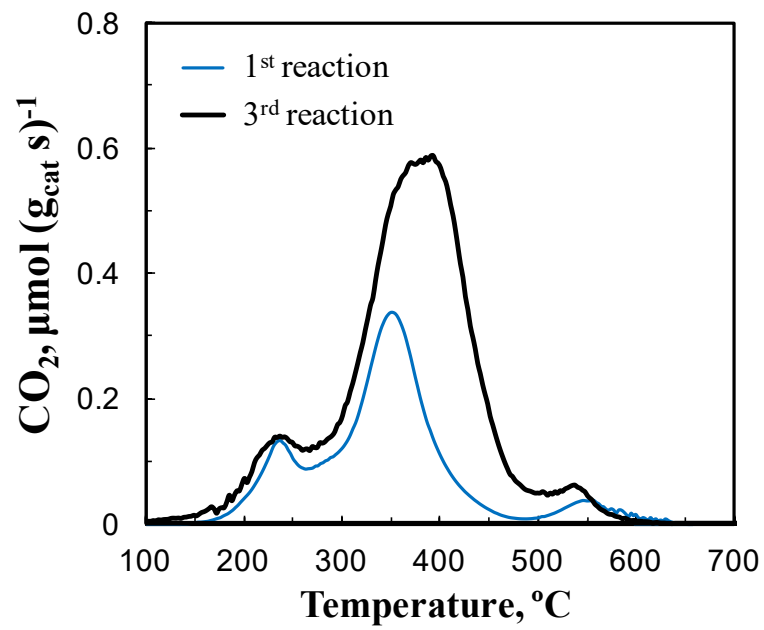
Figure 6
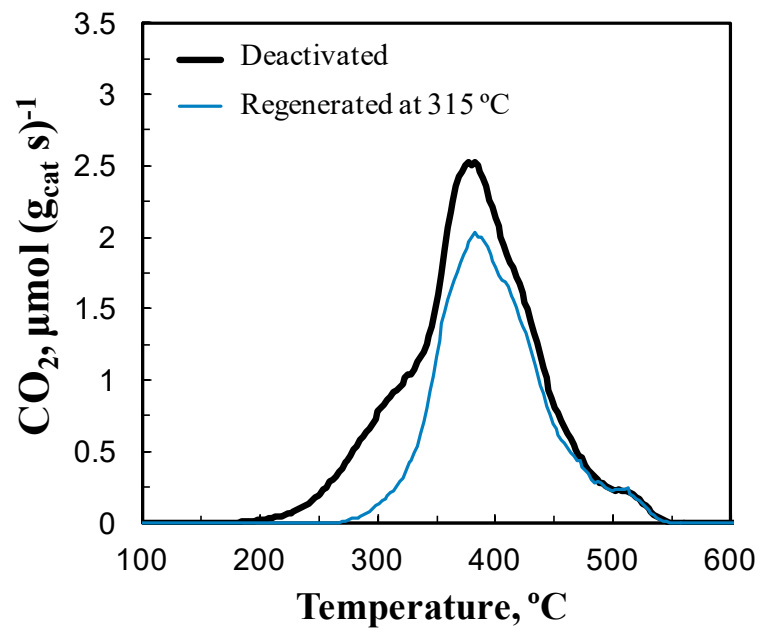
Figure 7
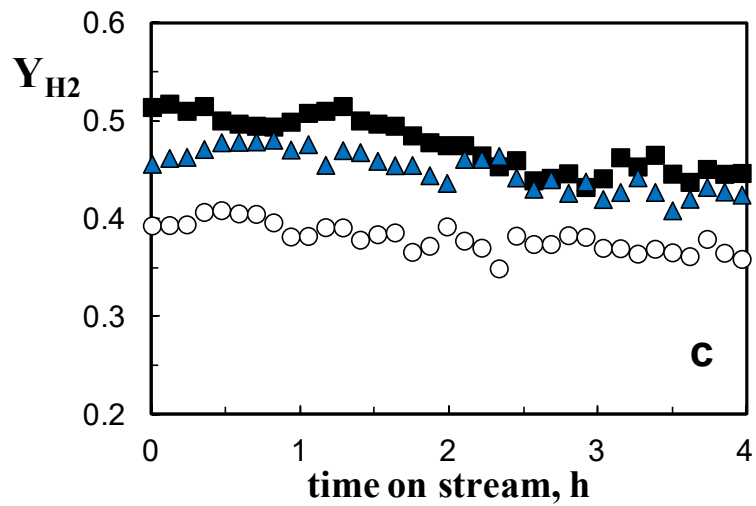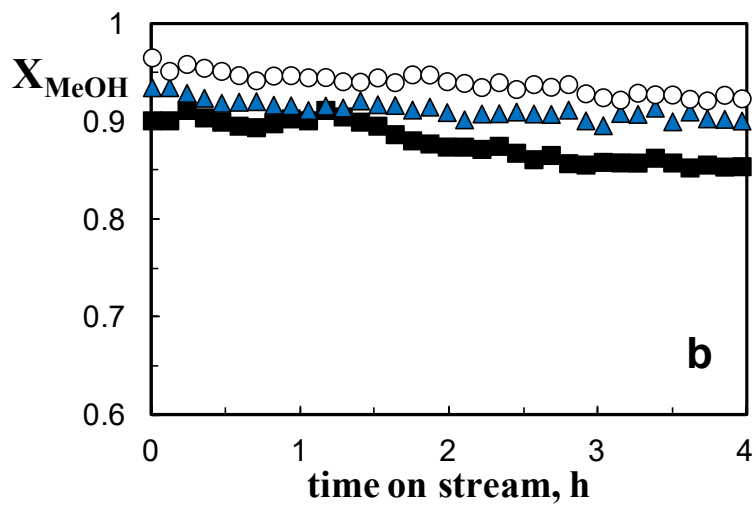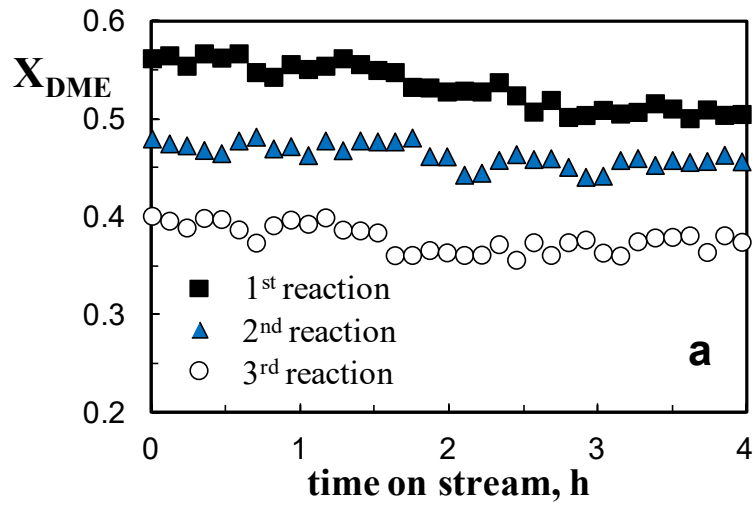
Figure 8
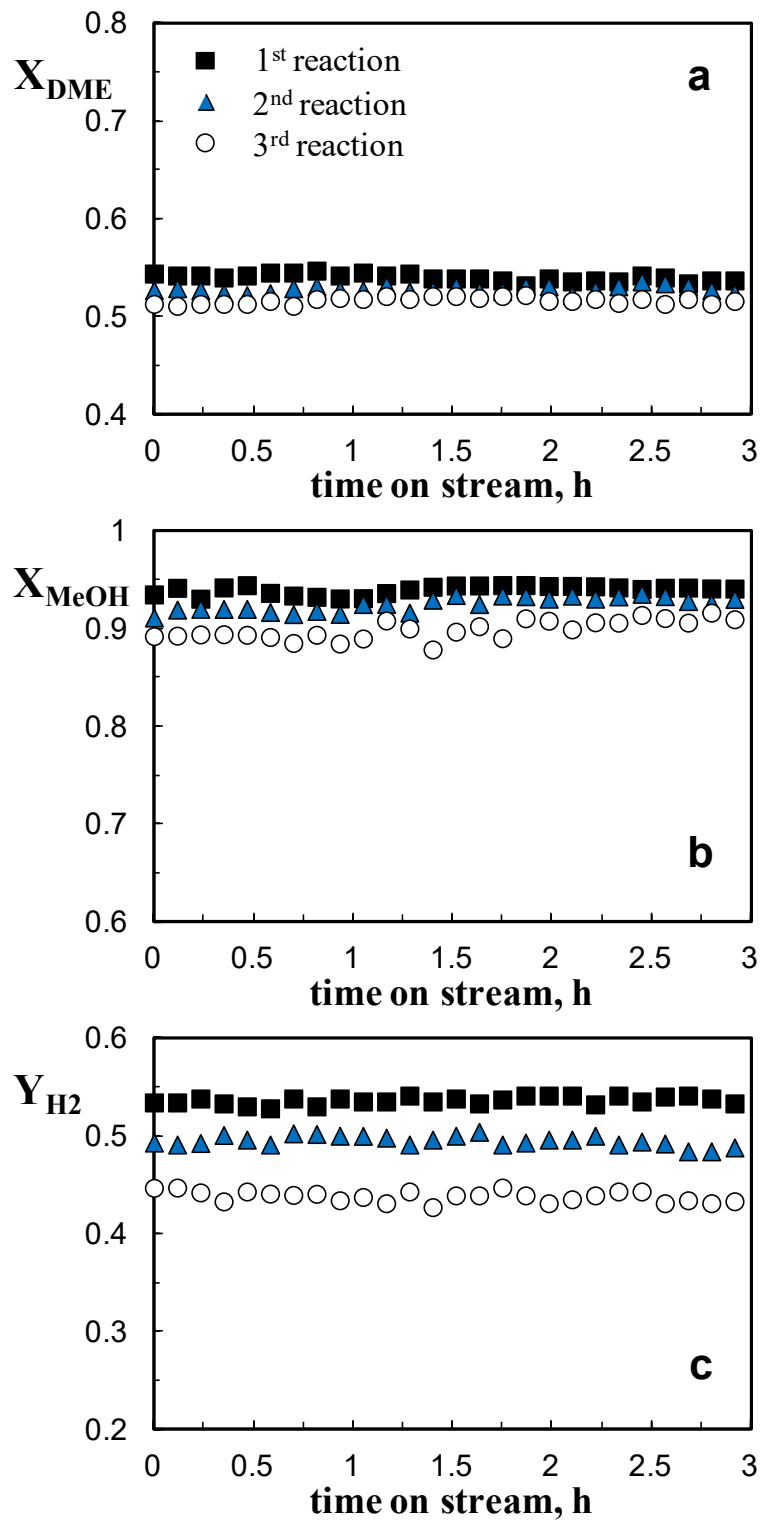
Figure 9
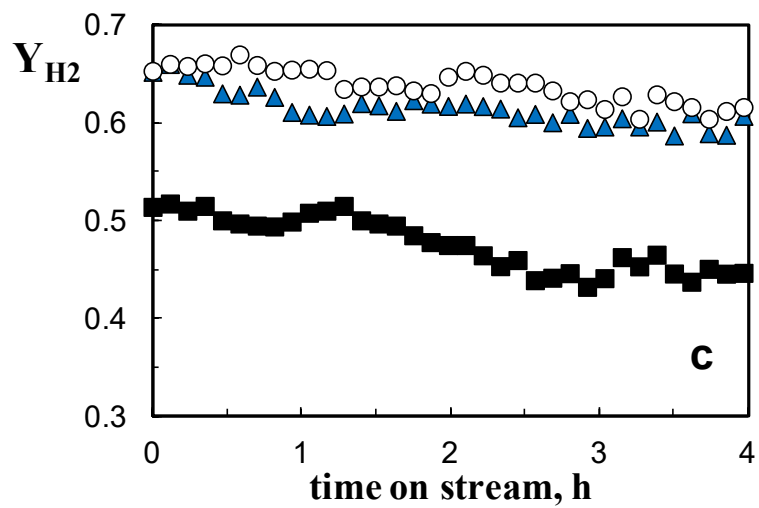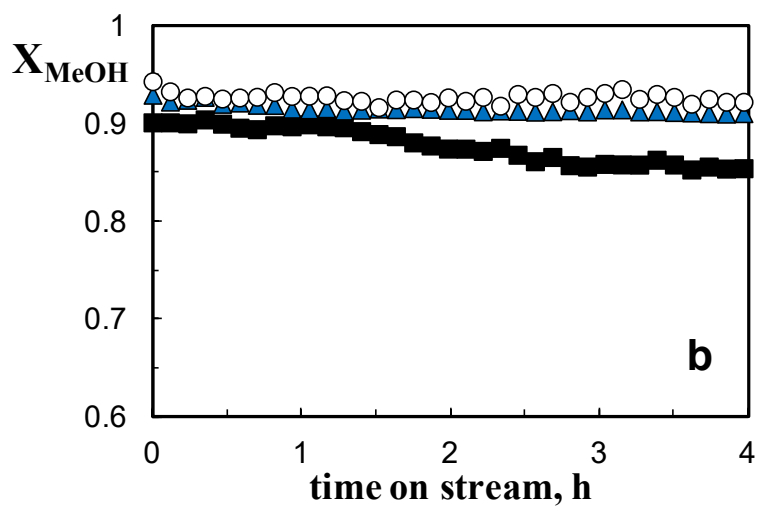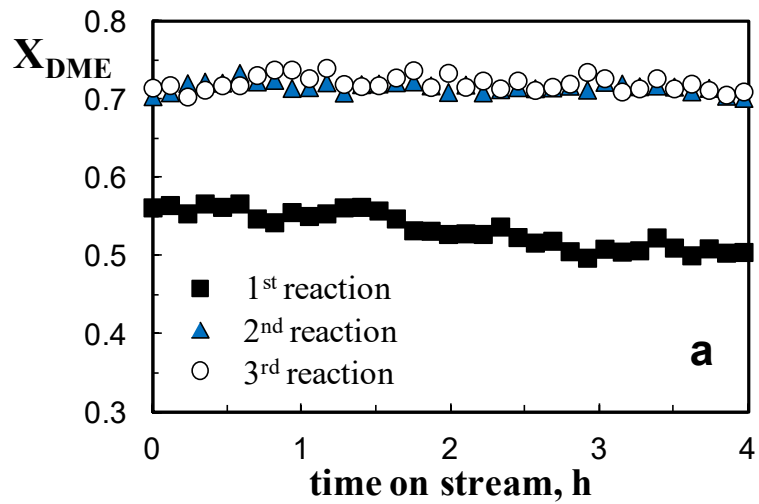
Figure 10

Table 1. Physical and chemical properties of the catalysts.

Property	CZA/AHZ30[1]	CZA/HZ30[1]	CuFe$_2$O$_4$/HZ30
S$_{BET}$, m^2 g^{-1}	207	230	81
V$_{micropore}$, cm^3 g^{-1}	0.041	0.057	0.025
V$_{mesopore}$, cm^3 g^{-1}	0.33	0.181	0.03
d$_{pore}$, Å	82	54	107
Total acidity, mmol NH$_3$ g^{-1}	0.34	0.44	0.24
Average acid strenght (DSC), kJ (mol NH$_3$)$^{-1}$	103	125	125
S$_{metallic}$, m$_{Cu}^2$ (g$_{Cu}$)$^{-1}$	56	56	5.8
D$_{metallic\ particle}$, nm	12	12	95

[1]Vicente et al. [14]